A PRELIMINARY FEASIBILITY ANALYSIS ABOUT THE STRUCTURAL HEALTH MONITORING OF RAILWAY CONCRETE SLEEPERS BY ACOUSTIC EMISSION AND DIGITAL IMAGE CORRELATION

Michele CARBONI[*], **Andrea COLLINA, Rui LIU, Emanuele ZAPPA**

Politecnico di Milano, Dept. Mechanical Engineering, Via La Masa 1, 20156 Milano, Italy

[*]Corresponding Author: michele.carboni@polimi.it

ABSTRACT

Railway concrete sleepers are made out of steel reinforced concrete and are a safety critical component of the railway track. Different kinds of failure are observed during service and this requires a maintenance plan involving non-destructive testing. Nevertheless, shifting from a non-destructive approach to structural health monitoring has shown relevant opportunities to increase in-service reliability and to decrease the costs of maintenance. From this point of view, the present paper describes a preliminary feasibility analysis about the application of acoustic emission for detection of cracks in prestressed concrete sleepers. For the purpose of assessment, obtained results are compared with other methods, such as digital image correlation and visual testing. Encouraging results indicate the possibility to carry out more validating tests in order to get the engineering of a suitably cheap monitoring system for in-service applications.

KEYWORDS: structural health monitoring, railway concrete sleepers, acoustic emission, digital image correlation

1. INTRODUCTION

Railway sleepers are that part of the track that transfers train loads from the rails to the ballast, keeping the correct gauge between the rails and their inclination. For safety purposes, it is required they shall withstand mechanical interactions and environmental aggressions. Wooden sleepers, concrete sleepers and, for a limited extent, steel sleepers are used. Nevertheless, prestressed concrete sleepers (Fig. 1) are the most common type in railway networks: they are extensively used for high speed tracks. They are characterized by several advantages:

- their weight, about 200-300 kg, is exploited to improve stability of continuous welded rail tracks;
- longer expected service life (50 years) with respect to timber sleeper;
- higher flexibility in terms of design;
- simplicity in manufacturing.

Anyway, they show some drawbacks, as well:

- high stiffness of the surface in contact with ballast, leading to higher rate of ballast crushing, with respect to timber sleeper;
- higher sensitivity to damage due to tamping machines.

Fig. 1 Examples of prestressed railway sleepers.

Failures of railway sleepers are related, along with the mechanical properties of the chosen materials, to the internal stresses generated by the loading conditions. The latter depend on the rail set and the ballast response. In particular, the dominating stress condition is, generally, represented by bending moments, able to cause the progressive cracking of the sleeper and typically due to a non-uniform distribution of ballast under the sleeper [1], and by impact loadings [2]. The most critical regions of concrete sleepers are the mid-span region and the rail-seat one: both may be interested by high bending moments and the possible presence of inherent flaws might accelerate the onset of damage and the consequent failure. It is also worth noticing different levels of dynamic loads are usually superimposed, worsening the scenario. Finally, the failure of concrete sleepers is more related to cumulated damage than singular extreme events: a stronger sensitivity to high magnitude and low cycle fatigue conditions, with respect to low magnitude and high cycle fatigue, is highlighted.

Since sleepers are safety critical elements, several standards are available in the European framework: EN 12350 (Testing fresh concrete), EN 12390 (Testing hardened concrete), EN 12504 (Testing concrete in structures), EN 12620 (Concrete aggregates) and EN 13230 [3] (Railway applications – Track – Concrete sleepers and bearers). The last one, between others, defines the experimental tests to be carried out on finished products for homologation. Basically, tests are carried out suitably loading full-scale specimens in order to generate bending moments. Three different kinds of tests are described: i) static bending test; ii) dynamic bending test, in which a dynamic load condition is applied in order to simulate impact load and cyclic loads; iii) (optional) fatigue bending test, in which a fatigue loading condition is provided. Each of these tests should be carried out at the mid-span region and at the rail-seat one.

Today, the methodologies for the in-service inspection of concrete sleepers, each characterized by peculiar advantages and drawbacks, consist in manual or automated visual testing, tap testing, x-rays and modal data analysis. For all these methods, the policy follows the protocol of the so-called "inspection interval based maintenance". Nevertheless, a limited number of in-service failures still occurs. If specific causes related to a combination of site condition and high axle load exist, the percentage of cracked sleepers can be rather large, ranging from 5% up to 15% or even more [4]. On the other hand, Structural Health Monitoring (SHM) draws its origins on the need of preventing catastrophic failures in different fields. The idea is to identify and monitor developing damages before their evolution in structural collapse, thus to guarantee and improve the safety and reliability of different systems. In particular, the application of SHM to the aerospace and civil fields has shown the possibility to reduce the cost of the in-service maintenance of structures by a maximum of 30% along with an improved reliability. Between the SHM methods under study for concrete sleepers, acoustic emission [5] and ultrasonic guided waves are available in the literature.

The present paper describes a preliminary feasibility analysis about the application of acoustic emission for detection of cracks in prestressed concrete sleepers. For the purpose of assessment, obtained results are compared with other methods, such as digital image correlation [6], used to quantitatively define the crack opening, and visual inspection. Encouraging results indicate the possibility to carry out more validating tests in order to get the engineering of a suitably cheap monitoring system for in-service applications. It is worth mentioning that the proposed approach enables to detect cracks also in the portion of the sleeper not visually accessible, i.e. lower surface or lateral surfaces, surrounded by ballast.

2. EXPERIMENT

A RFI 260 type prestressed concrete sleeper was tested in the lab, in correspondence of the mid-span section (Fig. 2), by a three point bending static load defined according to [3] as "static bending test". During the test, non-destructive testing and SHM were carried out by visual testing, acoustic emission (AE) and 2D digital image correlation (DIC).

Components: 1 rigid support, 2 articulated support, 3 resilient pad, 4 sleeper.

| (a) | (b) |
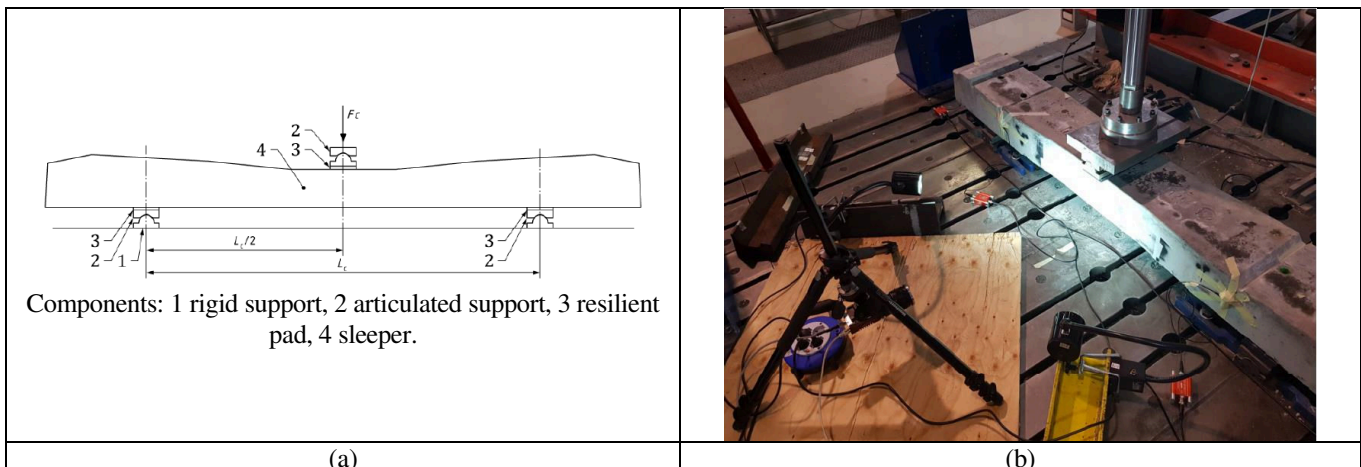
Fig. 2 Three-point bending static test of a railway concrete sleeper: a) scheme of the loading set-up; b) set-up.

A 300 kN servo-hydraulic actuator, controlled in force, was employed. Two articulated supports were placed under the sleeper at the distance prescribed by the standard. In order to avoid crack generation and propagation at supports, rubber pads, one for each support, were used; they also provided a better load distribution at contact surfaces. An articulated support and a rubber pad were also used at the application point of the load generated by the actuator. The time-load history prescribed by the standard for the static bending test is shown in Fig. 3a: in the very first part, load is increased, with a maximum rate of 120 kN/min, up to the F_{c0} value defined by the standard itself according to sleeper size. Then, sequential increments of 5 kN are applied, interspersed by time intervals lasting from 10 s to 5 min, up to F_{cr}, i.e. the load value producing the first visible crack. Finally, further load increments are prescribed up to the ultimate load value F_{cb}. Since the aim of the work was not to carry out the homologation of the sleeper, load was here kept increasing (Fig. 3b) up to the total catastrophic destruction of the sleeper.
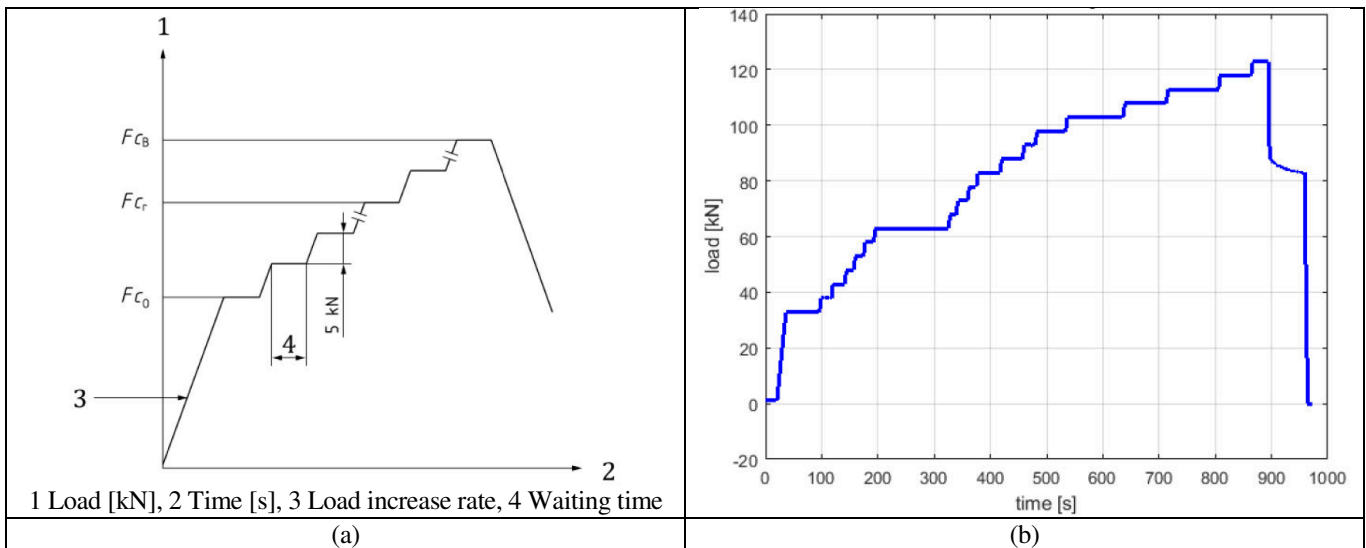
Fig. 3 Time-load history for the static bending test: a) standard prescriptions; b) applied one.

AE was carried out by a Vallen Systeme AMSY-6 control unit with eight channels and by applying six sensors to the sleeper (Fig. 4): two at the lateral extremities and the other four closer the region of interest, i.e. the region where cracks are supposed to appear. Coupling of sensors to the concrete surface is obtained by means of a silicon couplant, while their slippage and detaching is avoided by taper. The measurement chain, for each of the adopted channels, was constituted by one AE piezoelectric sensor (Vallen VS150-M with resonance frequency equal to 150 kHz) linked to a preamplifier (AEP4 34 dB) leading to the ASIP-2, a dual channels AE-signal processor card. The sample frequency was set to 10 MHz, while the acquisition threshold (40 dB) was defined on the base of the HSU-Nielsen pencil response, which allowed the calibration of the sound velocity in the tested concrete sleeper (3320 m/s), as well. No filtering was applied to the recorded signals.
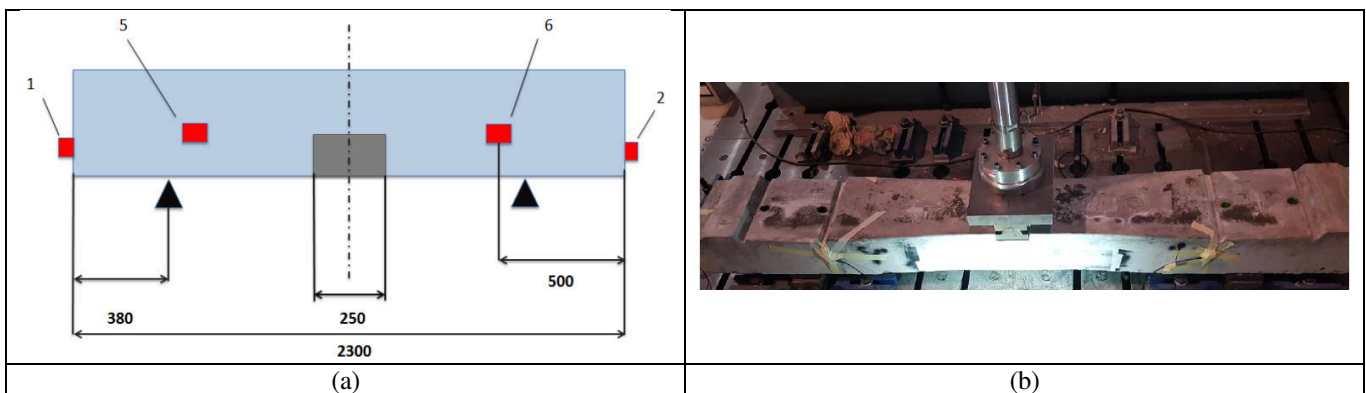

Fig. 4 AE set-up: a) schematic representation; b) application by taper.

During the test, the initiation and propagation of cracks was inspected by means of visual testing. Visual inspection was performed by means of digital microscope Dino-Lite AM4113/AD4113 connected to an external PC. It was thus possible to record images with a 20x magnification and an accuracy of 0.01 mm.

In order to improve damage evaluation during the test, 2D DIC was applied. Images were recorded by means of a GX3300 digital camera equipped with a Zeiss lens of 50 mm optical length. The camera was mounted on a tripod in the front of the sleeper, to face the area where cracks were most likely to appear (Fig. 2b), and was connected to an external PC controlling the camera itself by means of a custom software developed in National Instruments LabVIEW environment. Since good lighting conditions were required, two LED lamps were used. A camera calibration procedure was carried out in order to compensate for perspective distortion and to define the conversion scale from pixel to [mm] (0.083 mm/pixel). The region of interest was speckled (Fig. 5) by an airbrush, a compressor and black opaque paint. To create a controlled speckle size and distribution, a chemically machined steel plate was used as a stencil. The feature pattern of the obtained speckle is characterized by an average diameter of 3-5 pixel and a coverage factor of 40%-70%: which is in the range of optimized speckle size for DIC.

**Fig. 5** Speckled region of interest of the tested sleeper.

(a)   (b)

(c)
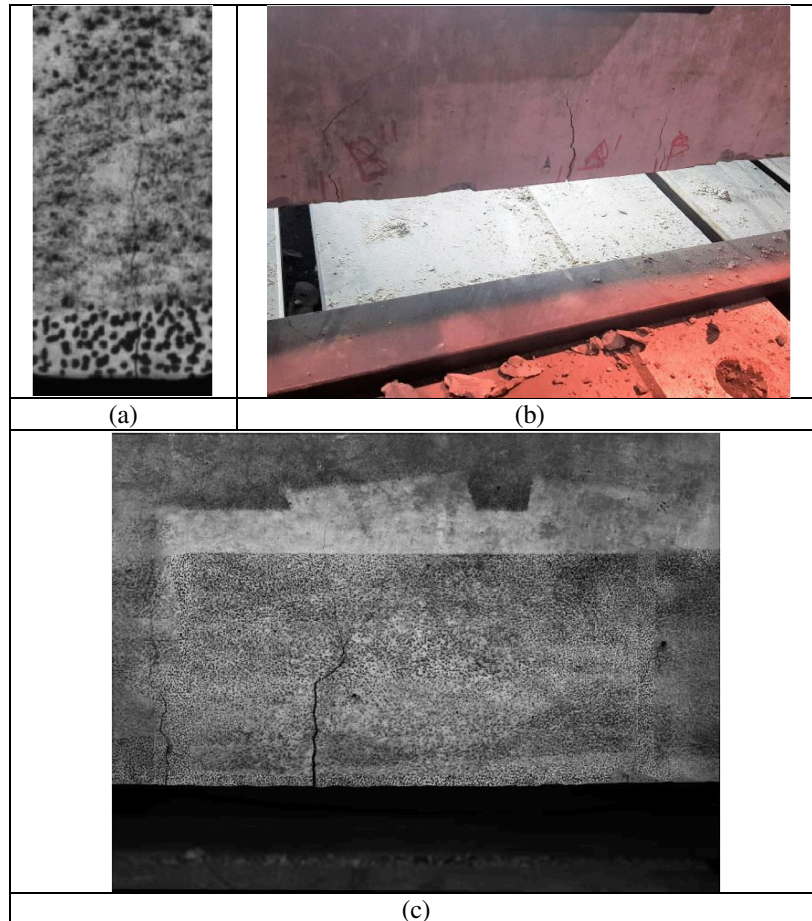
Fig. 6 Initiation and propagation of cracks during the test: a) at 62.9 kN; b) .at 72.9 kN; c) at 97.9 kN.

3. RESULTS AND DISCUSSION

The very first visible crack was recorded at a load level of 62.9 kN (Fig. 6a) on the side of the sleeper monitored by the DIC camera. As expected, the crack appeared in the region around the centerline of the sleeper. Increasing the load, at 72.9 kN both sides of the sleeper begin to show multiple cracks (Fig. 6b), while at 97.9 kN such cracks tend to reach the neutral axis of the sleeper on each side. The test finished at 122 kN, when the sleeper failed completely.

Fig. 6 highlights that small cracks can be rather tough to be detected by visual testing, because the conditions of the inspected surface, especially considering in-service sleepers, might be prohibitive. The same does not hold for DIC, where the detection of the crack can get a higher accuracy. Indeed, at each increment of load, a picture of the speckled area was taken by the camera; this resulted to be very useful, especially, in post-processing of AE data. Each picture was used to define the local strain field by correlation to the reference picture taken at 0 kN load level. Image processing was carried with the software VIC 2D by Correlated Solutions. Since DIC allows to estimate the displacement and strain fields of the specimen in the field of view, the information is not limited to a portion of the sleeper, but it covers the region where the main crack is likely to produce. In particular, to detect the crack path, the strain field is considered. Fig. 7 shows some examples of DIC results, in terms of the maximum principal strain, for two cracks at different applied loads. As can be seen, the crack path is clearly visible in the strain map. It should be noted that the strain values visible in the figure are not representative of real strain (since along the crack the concrete obviously shows a discontinuity) but are rather apparent strain due to the output of the numerical differentiation used to estimate the strain field from the displacement one. Nevertheless, the very large apparent strain values allow to detect the crack path even in the case of extremely low crack opening. This allows to early detect the crack, when the opening is of the order of a few micrometres: well before it is visible by the operator. As the loading increases, more cracks can appear (see Fig. 7b, c and d) and crack bifurcations can happen: all these phenomena can be measured processing the strain field estimated with DIC.
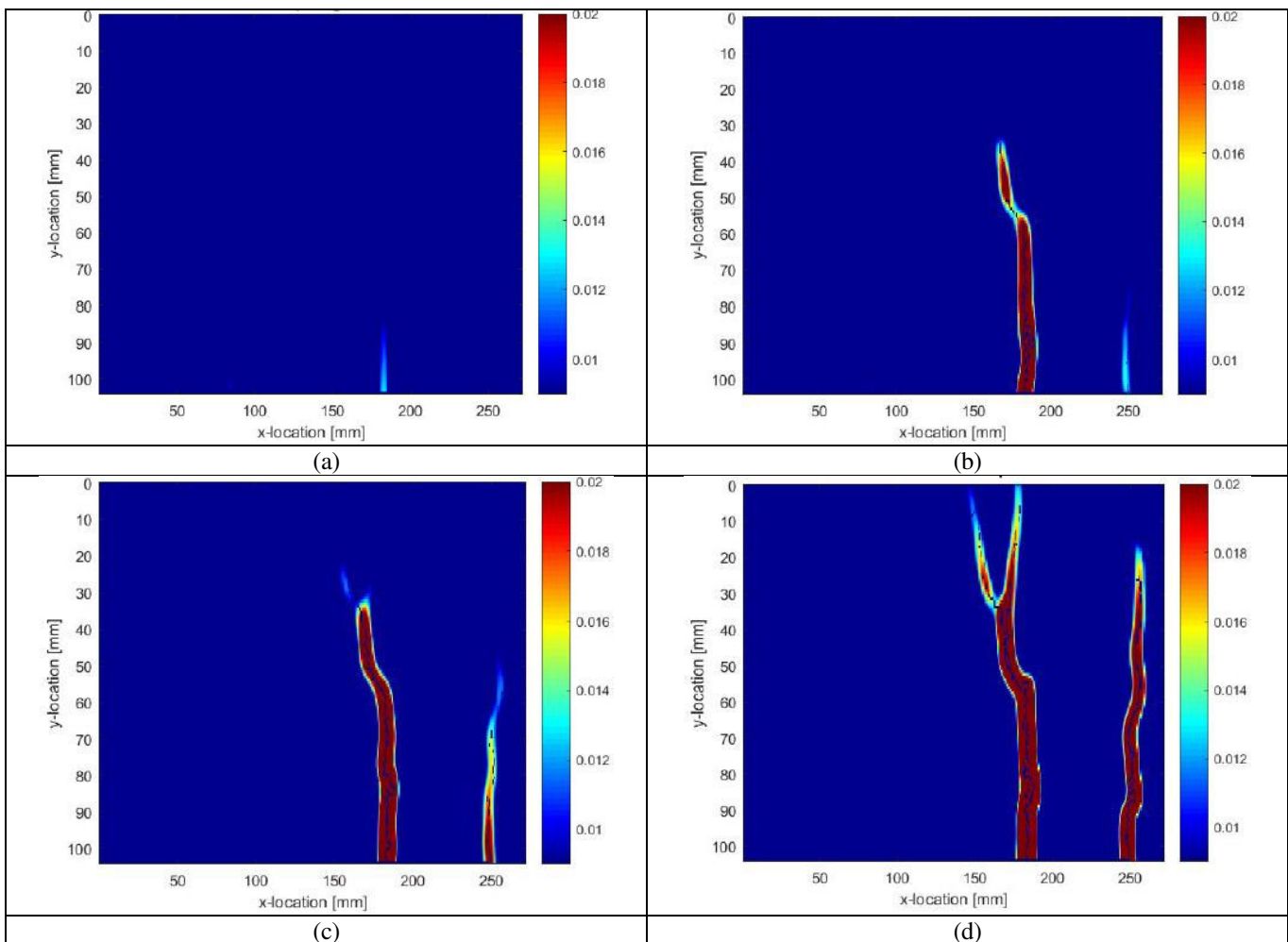

Fig. 7 Examples of DIC results, in terms of the maximum principal strain, for two cracks at different applied loads: (a) 72 kN; (b) 92 kN; (c) 97 kN; (d) 107 kN.

Regarding AE results, what it is possible to state is that, by increasing the load, the acoustic activity increases and the same holds for the amplitude and the energy of the hits. From this point of view, Fig. 8 depicts AE activity in terms of amplitude and cumulated energy for channel 1, located at one extremity of the sleeper. The observed trend of AE activity is coherent with the physical phenomenon: indeed, anytime a crack is formed or increases its dimensions, AE events, amplitude and energy are generated. This is also confirmed by a comparison to DIC results (Fig. 9, where the cumulated energy of AE activity and the length of the two cracks shown in Fig. 7 are reported). Despite the two methods (AE and DIC) have a different nature, being volumetric and local techniques respectively, it is possible to find a correlation: to an increase in size of the crack, it is possible to observe an increase of the AE activity, cumulated energy and amplitude. In this case, however, it is not possible to associate the overall increment just to the development of the examined crack. Nevertheless, the application of DIC allows to understand the origin of a portion of the AE activity.

(a)   (b)
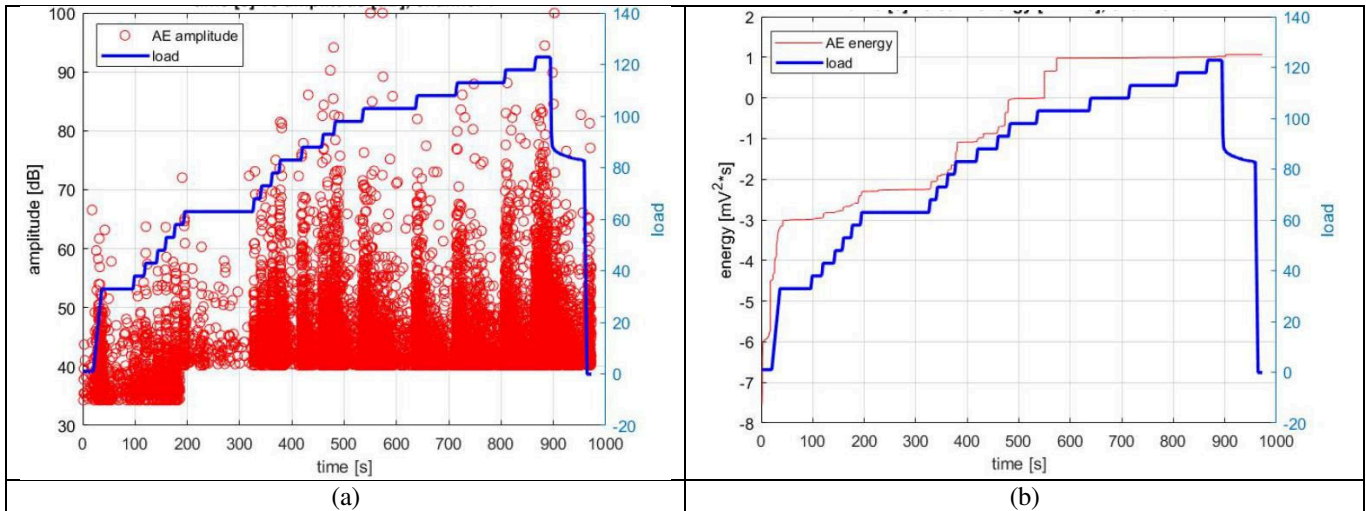
Fig. 8 AE activity recorded by channel 1: a) amplitude of AE events and load history vs time; b) logarithmic cumulated energy of AE events and load history vs time.


(a)   (b)
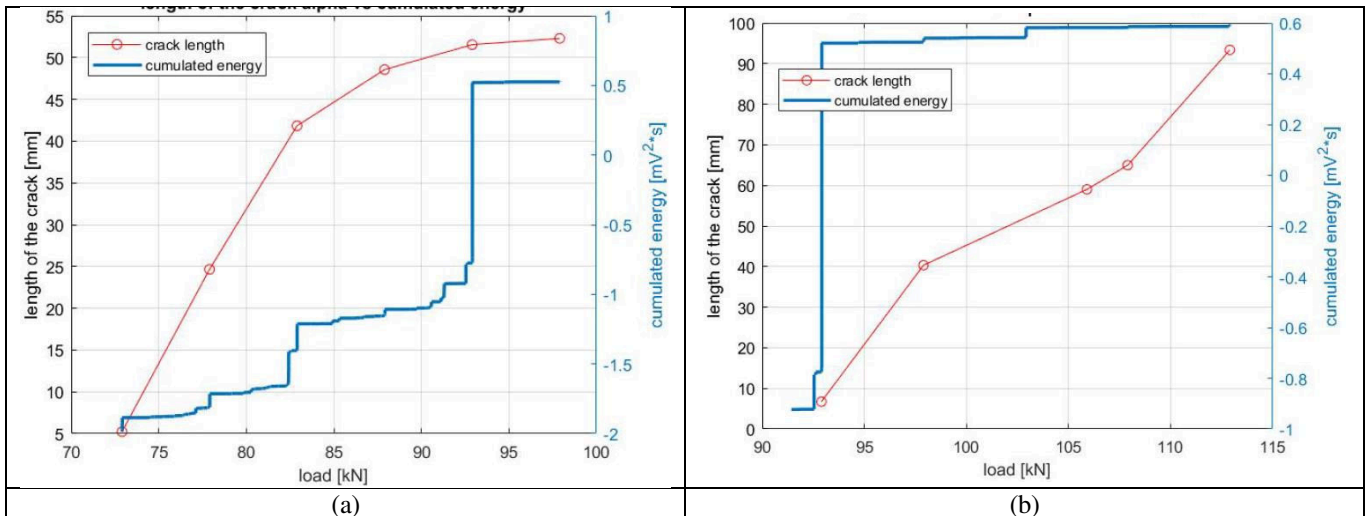
Fig. 9 Crack length and cumulated energy (in logarithmic scale) vs. load: for the two cracks shown in Fig. 7.

Even if providing some useful and interesting information, the AE results shown up to now refer to the total amount of recorded data: it is reasonable to expect part of such data is not directly related to damage phenomena, but to different types of noise and interference, such as electro-magnetic noise, the action of the servo hydraulic cylinder, friction at constraints, etc. In light of this, a more detailed analysis of the results was conducted by means of pattern recognition tools based on data clustering exploiting unsupervised artificial neural networks, Self-Organizing Maps and K-means algorithm (all implemented by dedicated Matlab scripts). In particular, higher emphasis is put in the research of those signals related to the brittle fracturing of the sleeper, i.e. the so-called "bursts".

6

There exists a wide literature devoted to the selection of the most significant parameters describing the waveform of AE signals, even if most of the research activity is addressed to the classification of the fracturing mode and not to the separation of bursts from all the other signals. In the present research, each AE event was recorded in terms of its full waveform in order to have the best flexibility for the analysis of the phenomenon. On the other hand, there is quite long list of available parameters to choose: amplitude, duration, energy, RMS, counts, peak frequency, centroid and so on. Just two parameters were here chosen: amplitude and variance because burst signals are characterized by a significant high amplitude, which explains the choice of amplitude, and by a short rise time and a more or less slow decay time, which explains the choice of variance.

The clustering process of the AE events lead to the identification of four main clusters. Fig. 10 shows, as an example, the results for channel 1 in terms of amplitude. In this particular case, on a total of 15993 recorded AE signals, 15740 fell in cluster #1, 3 in cluster #2, 32 in cluster #3 and 218 in cluster #4.
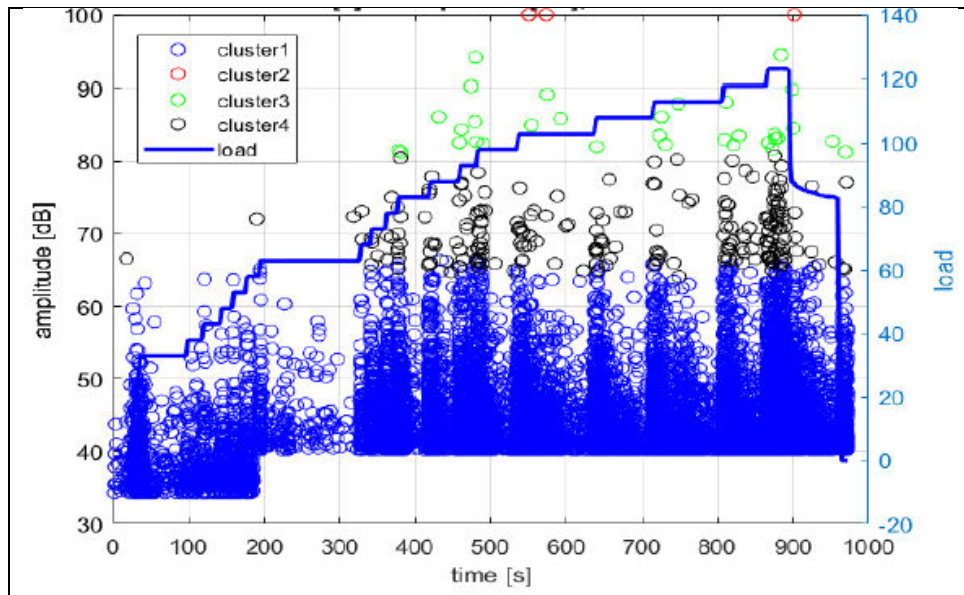

Fig. 10 Results of the clustering of AE events (in terms of amplitude) vs. load for channel 1.

The first clue is that just cluster #1 was identified for the applied load levels lower than 62.9 kN, when the first visible crack was observed. This seems to suggest cluster #1 contains the noise, while clusters #2, #3 and #4 contain AE events related to damage evolution. In order to deepen the nature of the signals belonging to each cluster, an investigation of the waveforms was carried out. Fig. 11 shows some examples of the waveforms included in cluster #1: as can be seen, these signals actually present waveforms very far from those expected for a burst, supporting the hypothesis it is the "noise cluster". It is also worth noticing cluster #1 represents about the 98% of all the acquired data, highlighting most of the experimental effort (acquisition, data storage, post-processing computational time, …) is devoted to meaningless signals. A possible future development of the research is, then, an optimization of the experimental parameters in order to lower the number of useless acquisitions.
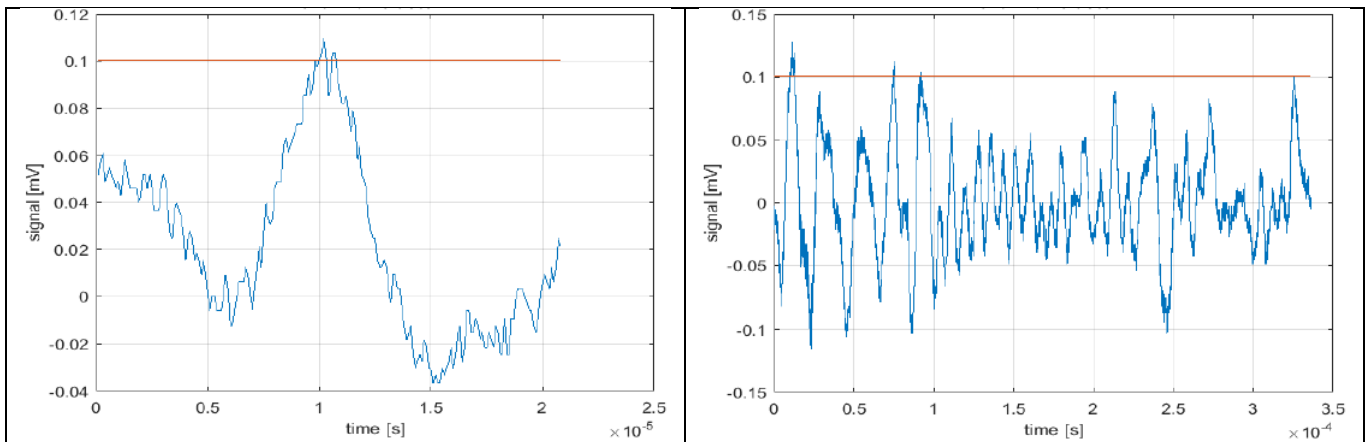
Fig. 11 Examples of waveforms belonging to cluster #1 of channel 1.

7

Fig. 12 shows, instead, some examples of the waveforms included in cluster #2, #3 and #4 of channel 1: as can be seen, these signals actually present the waveform expected for a burst. Nevertheless, the physical meaning of the signals included in these three clusters seems to be the same and, consequently, they should be represented by just one cluster. This can be explained noting that the results of clustering by unsupervised artificial neural networks do depend on the nature of the signals and the parameters used to classify them, hence it is not possible to know a priori the number of needed clusters and the kind of signals they include. In the present application, the subdivision of the bursts into three clusters reflects the fact that, although being bursts, these signals have an amplitude and a signal to noise ratio very different in the three clusters. An optimization of the post-processing procedure in order to avoid the distribution of similar signals into different clusters is an open point of this research.
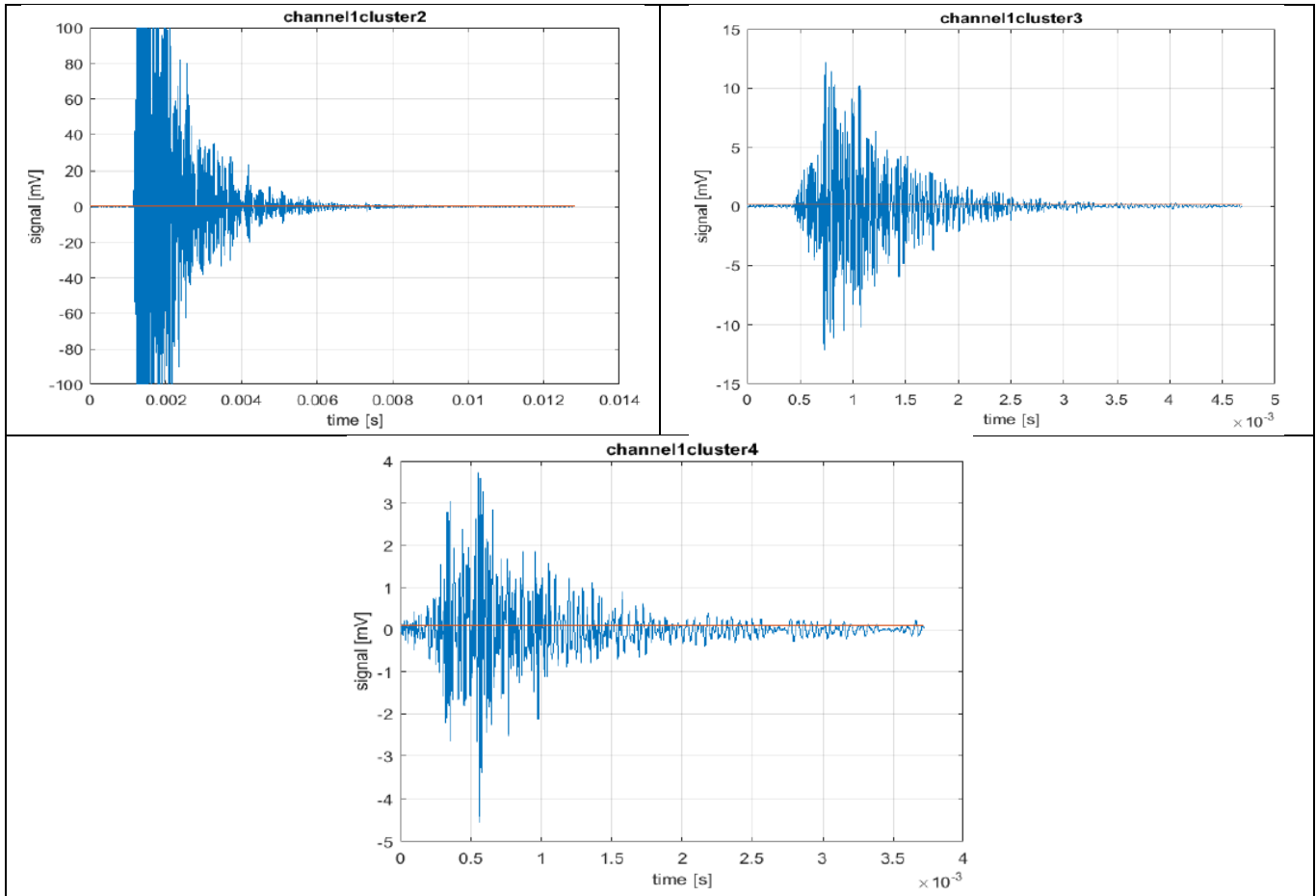

Fig. 12 Examples of waveforms belonging to cluster #2, #3 and #4 of channel 1.

Another interesting diagram of the results of the clustering process is the one drawn in the amplitude-variance plane (Fig. 13a) because it makes easier their interpretation and adds information with respect to the one shown in Fig. 10. In this sense, it is possible to understand how the dimensionality of the parameters used to classify the data and their dispersion in the plane amplitude-variance play a role in the clustering process. Such a diagram is here reported for channel 1, but the same trend can be observed for the other channels. It has to be highlighted the nearly linear trend of data and the fact that the clusters related to bursts (#2, #3 and #4) are systematically distributed in regions of higher amplitude an variance with respect to the cluster of noise (#1).

A final way to investigate the nature of the clusters is represented by the graph of the energy cumulated during the test, especially useful when the amount of recorded AE events gets huge. Fig. 13b depicts the diagram of the cumulated energy of each cluster in the case of channel 1. It is possible to observe that the most significant and the steepest energy increments are classified into the clusters of bursts, even if the number of signals included in these clusters is just the 2% of the total amount of recorded signals. It is clear that clusters of bursts are those with higher energy content. Moreover, the trend of cluster #1 is nearly linear, suggesting the presence of continuous emission of noise over time, without instantaneous releases of energy typical of a brittle fracturing phenomenon. The same reasoning can be extended to all the other channels.
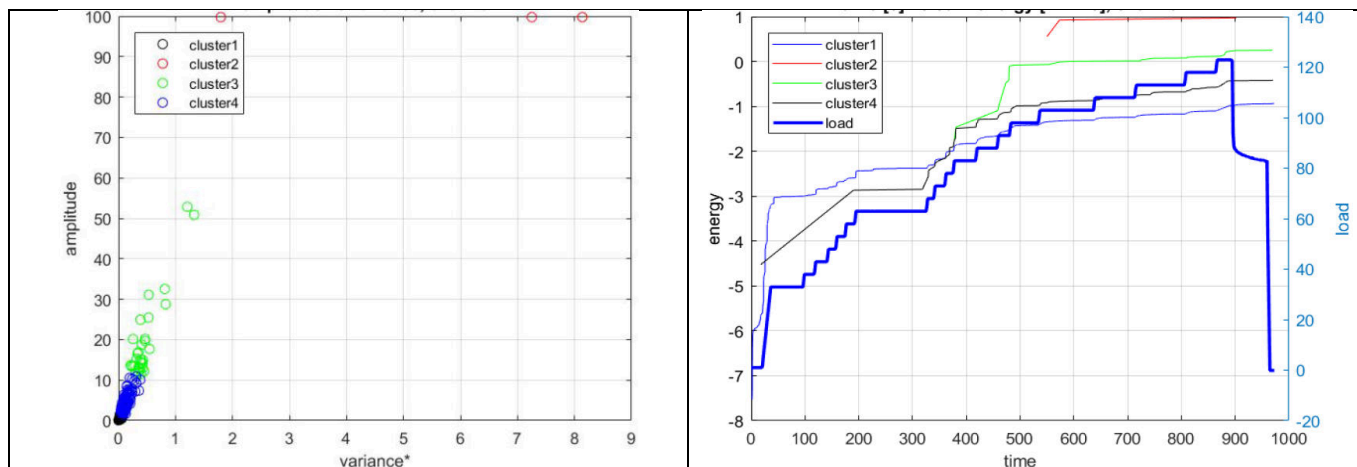
Fig. 13 Results of the clustering of AE events for channel 1: a) amplitude-variance diagram; b) cumulated energy of all the clusters vs. load.

4. CONCLUSION

A preliminary feasibility experimental analysis about the structural health monitoring of railway concrete sleepers, carried out by acoustic emission and digital image correlation, provided encouraging results. The next steps consist of carrying out more static and dynamic tests in order to check the repeatability of the methodology and the design and engineering of a suitably cheap monitoring system for in-service applications.

ACKNOWLEDGMENTS

REFERENCES

[1] C. Esveld, Modern railway track, II Ed., MRT Productions, Zaltbommel, ISBN: 978-1-326-05172-3, (2016) 241.
[2] S. Kaewunruen, A.M. Remennikov, Progressive failure of prestressed concrete sleepers under multiple high-intensity impact loads, Eng. Struct., 31 (2009) 2460-2473.
[3] Railway applications-track-concrete sleepers and bearers-Part 2: prestressed monoblock sleepers, European Standard, EN 13230-2.
[4] C. Gonzalez-Nicieza, M.I.A. lvarez-Fernandez, A. Menendez-Dıaz, A.E. A lvarez-Vigil, F. Ariznavarreta-Fernandez, Failure analysis of concrete sleepers in heavy haul railway tracks, Engineering Failure Analysis 15 (2008) 90–117.
[5] M. Ohtsu, Acoustic Emission and Related Non-destructive Evaluation Techniques in the Fracture Mechanics of Concrete, Woodhead Publishing Series, 2015.
[6] M.A. Sutton, J.J. Orteu, H.W. Schreier, Image Correlation for Shape, Motion and Deformation Measurements, Springer Science+Business Media, 2009, ISBN: 978-0-387-78746-6.